Experimental investigation on mechanical behavior of sands treated by enzyme-induced calcium carbonate precipitation with assistance of sisal-fiber nucleation

Jianwei Zhang, Yue Yin, Lei Shi*, Hanliang Bian and Wanpeng Shi

School of Civil Engineering and Architecture, Henan University, Kaifeng, China

Sisal fibers had obvious advantages of mechanical strength on reinforced enzyme-induced calcium carbonate precipitation (EICP)-cemented loose sands. However, there are few related researches, whose research on strength and toughness is not sufficient, and the analysis on mechanism is lacking. In this article, sisal fiber was used to strengthen EICP-treated sand, and the mechanical properties and underlying mechanism were experimentally explored. The results show that the strength and toughness of EICP-treated sand can be effectively improved by sisal fibers. The optimal sisal fiber length is 10 mm and the optimal fiber content is 0.2%. The wet-dry cycle resistance of the samples is improved simultaneously. Microscopic study showed that the rough surface of sisal fiber provided a large number of nucleation sites for calcium carbonate precipitation and formed an effective "bridge network." This study reports the potential and the underlying mechanism of sisal fiber on improvement of EICP performance by new test methods and provides new insight into enhancing mechanical behavior of EICP-cemented loose sands with natural fiber.

KEYWORDS

sisal fiber, enzyme-induced calcium carbonate precipitation, sand, strength, toughness, wet-dry cycles

1 Introduction

Construction of the Sichuan–Tibet railway faces many technical problems, such as strong tectonic motion, large altitude differences, frequent earthquakes, complex geological conditions, seasonally frozen soil, hazardous mountain slope sliding, plateau hypoxia, and ecological environmental protections (Allen et al., 2019; Song et al., 2021; Zhang D. et al., 2022). Loose sand in some areas has poor engineering properties, which may induce sandstorms and landslides, threaten engineering safety (Wang et al., 2021). Using technical methods to solidify sandy soil can effectively improve

the safety of related regional engineering (Carmona et al., 2018; Wang et al., 2020; Yao et al., 2021). Enzyme-induced calcium carbonate precipitation (EICP) technology is regarded as an environmentally friendly sand treatment method (Phillips et al., 2013; Almajed, 2017; Hamdan, 2019; Tang et al., 2020; Jiang et al., 2021).

The principle of enzyme-induced calcium carbonate precipitation (EICP) technology is to extract urease from plants and promote the hydrolysis of urea to carbonate ions (Hamdan et al., 2013). Carbonate ions combine with calcium ions in the environment to produce calcium carbonate (DeJong et al., 2006). Because this technology is green and effective, it has a broad application prospect in soil reinforcement (Neupane et al., 2013), seepage prevention (Gao et al., 2019), dust control (Jiang et al., 2019; Sun et al., 2021) and other engineering fields (Tang et al., 2020). The effect of EICP treatment on sand has been proved (Wu S. et al., 2021), but the sand treated by EICP become typical brittle failure (Xiao et al., 2019). This is detrimental to the safety of the project. In addition, the nucleation site is one of the key factors affecting EICP treatment, but quartz sand can provide a limited number of nucleation sites (Cui et al., 2017). These reasons limit the use of this technology.

Pre-addition of fibers to sand is considered to be effective in overcoming the above shortcomings of EICP (Almajed, 2017). Fibers can provide effective nucleation sites for calcium carbonate generation (Fang et al., 2020). This results in higher strength of EICP-treated sand. At the same time, the addition of fibers can improve the toughness of EICP-treated sand (Li et al., 2016). Existing studies have confirmed the effectiveness of various fibers including basalt fiber (Xiao et al., 2019), PVA fiber (Choi et al., 2016), polypropylene fiber (Lei et al., 2020), glass fiber (Phillips et al., 2013) and carbon fiber (Qiu et al., 2019; Zhao et al., 2020a) in improving the strength and toughness of sand treated by EICP. Fiber type, fiber length and fiber content are the key factors affecting the treating effect (Choi et al., 2019; Xiao et al., 2019; Jiang et al., 2021). In general, after EICP treatment, the mechanical properties of sand with fibers are greatly improved, such as unconfined compressive strength, splitting tensile strength, residual strain and failure strain (Sharma et al., 2019; Zhao et al., 2020b). The conversion rate of calcium carbonate was also improved after fiber was added. The microscopic distribution of calcium carbonate is also more reasonable (Huang et al., 2020; Yao et al., 2021).At present, synthetic fibers are widely used in the field of soil reinforcement. Synthetic fibers are cheap and chemically stable (Hejazi et al., 2012). However, synthetic fiber is not degradable, which will cause environmental pollution when applied to engineering (Hao et al., 2018). Meanwhile, the production of synthetic fibers consumes a lot of energy and emits greenhouse gases (Ibraim et al., 2012; Minto et al., 2018). Natural fibers can also be used in EICP treatment (Almajed, 2017). Studies show that sisal fiber, hemp fiber, jute fiber, coconut shell fiber and wool fiber can be used

as reinforced materials of sand treatment (Pasillas et al., 2018; Qiu et al., 2019; Lei et al., 2020; Iamchaturapatr et al., 2022).

Sisal fiber is an ideal fiber with low price, abundant yield and environmental protection (Castoldi et al., 2019). Its mechanical properties are even better than synthetic fibers (Sharma et al., 2019). Compared with synthetic fibers, degradation of natural fibers is controllable, which is mainly reflected in the following two aspects. On the one hand, there are many modification methods to improve the long-term durability of sisal fiber (Kiran and Ramakrishna, 2019). On the other hand, sisal fiber in soil can achieve pollution-free degradation (Zhang J. et al., 2022; Mert Tezer and Başaran Bundur, 2022). Correspondingly, synthetic fibers are accompanied by the generation of pollutants in both the production and elimination process (Morán et al., 2008; Frazão et al., 2018; De Castro et al., 2021).

The studies of Amajed (2017) and Amajed et al. (2018) confirmed the effect of sisal fiber on EICP-treated sand. Those few studies on sisal fiber focus on the improvement of unconfined compressive strength and failure strain of EICP-treated sand by fiber content. For EICP-treated sand, these studies about strength and toughness are inadequate (Phillips et al., 2013; Carmona et al., 2018; Jiang et al., 2021). Stress-strain model, elastic modulus, elastic modulus at 50% of the unconfined compressive strength, residual strength, failure pattern, calcium carbonate content, crystal type other parameters should also be elaborated in the relevant studies of fiber-reinforced sand (Choi et al., 2016; Xiao et al., 2019; Fang et al., 2020; Tang et al., 2020; Lv et al., 2021). Besides, fiber length is an important parameter, but it is often ignored in previous studies (Almajed, 2017). Analysis of EICP solution will also help to understand the mechanism (Yao et al., 2021). In addition, natural fibers are made from cellulose and are biodegradable (Senthilkumar et al., 2018; Sharma et al., 2019). Wet-dry cycle test is helpful to understand the performance of natural fiber-soil composites under short-term environmental erosion (Ibraim et al., 2012; De Melo et al., 2019). This is the basis for exploring the life cycle durability of natural fibers in the future (Sharma et al., 2019). Nevertheless, most of the studies about EICP-treated sand reinforced by sisal fibers have ignored these aspects (Almajed et al., 2018).

The purpose of this study is to investigate the effects of sisal fiber length and content on stress and strain mode, unconfined compressive strength, failure strain, elastic modulus, elastic modulus at 50% of the unconfined compressive strength, residual strength, failure pattern and calcium carbonate content of EICP treated sand. The strength and mass loss of samples under the wet-dry cycles will be investigated simultaneously. In addition, the mechanism will be explained by solution analysis experiment and microscopic experiment. The main objective of this study is to explore more convincing ideas and to carry out further research to enrich the existing body of knowledge related to the application of EICP to sisal fiber reinforced sand.
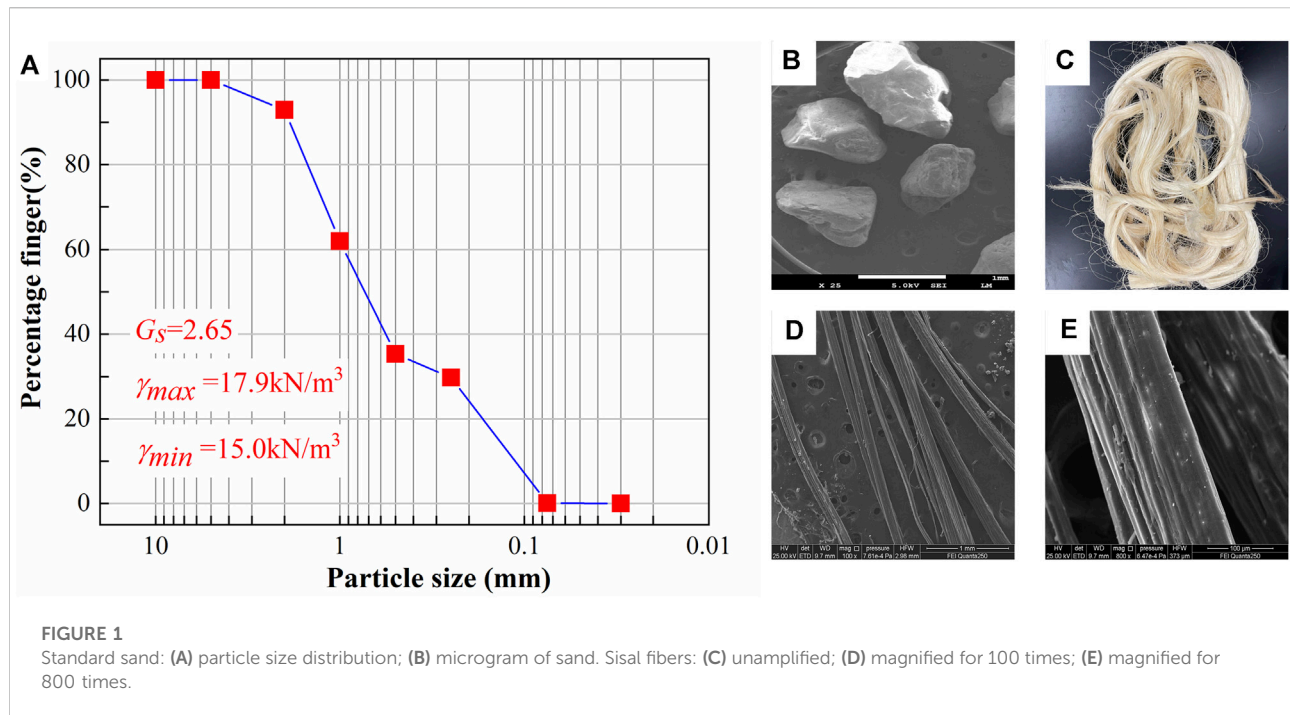
FIGURE 1
Standard sand: **(A)** particle size distribution; **(B)** microgram of sand. Sisal fibers: **(C)** unamplified; **(D)** magnified for 100 times; **(E)** magnified for 800 times.

TABLE 1 Physical parameters of the fibers.

Fiber type	Density/kg/m³	Elastic modulus/GPa	Tensile strength/MPa	Elongation after fracture/%	Diameter/mm	Moisture absorption rate/%
Sisal fiber	1,124	8.3	637	2.2	0.081	75

2 Materials and methods

2.1 Test materials

Chinese standard sand composed of quartz was used in this study. The specific gravity (G_s) of this sand was 2.65. The maximum dry weight (γ_{max}) of the sand was 17.9 kN/m³. The minimum dry weight (γ_{min}) was 15.0 kN/m³. The particle size distribution and microgram of this sand is shown in Figures 1A,B. The mean particle size (D_{50}) of the sand was 0.52. The curvature coefficient (C_c) was 1.05. The nonuniformity coefficient (C_u) was 2.2.

Sisal fibers, produced in Guangdong, were used in this study. Sisal fiber is light yellow in its natural state, as shown in Figures 1C,D,E show SEM images of sisal fibers at different magnifications.

Table 1 shows the physical properties of the sisal fibers used in this experimental study. The length of sisal fibers was cut to 5, 10, 15 and 20 mm (Li et al., 2016; Almajed et al., 2018; Lv et al., 2021). The fiber content (mass ratio of fiber to sand) was 0.1%, 0.2%, 0.3% and 0.4%. Previous studies have made some preliminary inquiries about fiber content (Li et al., 2016; Almajed et al., 2018; Lv et al., 2021). Based on those studies, we speculate that the optimal value of fiber content should be among 0.1%–0.4%.

2.2 Urease solution and cementing solution

Soybeans were dried, ground into powder, sifted by a sieve with a 2 mm aperture, and mixed with a certain amount to deionized water. The concentration of soybean powder was 10, 20, 30, 40, 50, 60, 70, 80, 90, 100, 150, 200 g/L (the ratio of soybean powder mass to deionized water volume). The soybean powder solutions were stirred on a magnetic mixer for 30 min and then put into a freezer at 4°C for 24 h. Next, each frozen sample was loaded into a centrifuge tube and centrifuged for

15 min at 3500 RPM. The obtained supernatant was the crude soybean urease solution (Khodadadii et al., 2020). The samples were stored at 4°C in a freezer for later use.

Urease activity was measured by a conductivity meter as follows. The urease solution was mixed with 1.11 M urea at a volume ratio of 1:9 and placed in a water bath at 30°C. The conductivity of the solution was measured every 5 min for 4 times (Almajed, 2017). The rate of change in the conductivity of the solution with time was calculated (Phillips et al., 2013). That is, the urease activity was expressed by the rate of change of conductivity in mM/min (Larsen et al., 2008b; Cui et al., 2021). The urease activity per unit mass was the urease activity divided by the weight of the soybean powder. The best concentration of soybean powder was selected for the sand solidification test by considering urease activity and urease activity per unit mass. A higher conversion rate of calcium carbonate was obtained when the cementation solution was 0.75 M (Carmona et al., 2018). The cementation solution was a mixture of 0.75 M urea and calcium chloride, which is the initial concentration (Sun et al., 2020).

2.3 Specimen preparation

The undercompaction moist-tamping method (Ladd, 1989) was used to prepare the sample. The samples were prepared at a warm room temperature of approximately 25°C. Deionized water is added to the sand to attain an initial moisture content of approximately 5%; then, dry fibers are manually mixed with the wet sand (Xiao et al., 2019). The water in the sand serves as lubricant and dispersant to avoid agglomerating the fibers (Ibraim et al., 2012). A sand column sample was prepared in a custom acrylic split two-lobe mold with a diameter of 39.1 mm and a height of 80 mm. The sand-fiber mixture is divided into five equal parts (Choi et al., 2019). Each part is carefully placed into the mold and compacted to a degree slightly greater than that of the underlying layer to obtain a more uniform density throughout the specimen (Xiao et al., 2019). The top of each layer is slightly scarified to avoid stratification among the layers. The bottom and top of the sample were provided with two layers of geotextile and a layer of fine sand to ensure that the solution could flow through the sand and that the sand particles would not be lost.

EICP treatment was realized by a peristaltic pump. Each sample was injected several times, first with urease and then with cementation solution. Both the urease solution and cementation solution volumes were 50 ml. The solution volume is about 1.5 times of the pore volume (Xiao et al., 2019; Lv et al., 2021). After an injection, the next injection was carried out after curing the sample for 24 h at room temperature. Next, the samples were cured at room temperature for 3 days after infusion. Then, residual impurities were removed by washing each sample with deionized water. The samples were dried in a drying box at 50°C for 24 h after the mold was removed. The number of treatments was 3 in the test. The initial dry density of the samples (before EICP treatment) was 1.606 g/cm³. At this point, it can be considered that the initial dry density of the sample is the same. Table 2 shows the experimental conditions in detail.

The optimal parameters of sisal fiber (fiber content and fiber length) can be obtained by analyzing the mechanical properties of each sample. The wet-dry cycles tests of EICP-treated sand reinforced with sisal fibers were carried out. EICP-treated sand without fiber was used as control. According to previous studies, the response of mechanical properties of EICP treated sand to wet-drying cycle can be observed by five wet-dry cycles (Liu et al., 2019). The number of wet-dry cycles are set as 0, 1, 2, 3, 4, and 5. Weigh the sample first during each wet-dry cycle. Then the sample was immersed in deionized water at an ambient temperature of 25°C. After 24h, the sample is taken out and placed in an oven at 50°C for 48 h. Then the unconfined compressive strength and mass loss of the samples after wet-dry cycles were measured. The strength loss ratio is the ratio of the strength lost (initial strength minus the strength after the wet-dry cycle) to the initial strength.

2.4 Test method

2.4.1 Unconfined compressive strength test

Unconfined compressive strength tests were carried out on a TSZ-10 testing machine. The loading rate was 1 mm/min, and data were recorded at 0.05 mm axial deformation intervals (ASTM D2166, 2013). The unconfined compressive strength is defined as the maximum value of the stress that can be reached for the stress–strain curve of the sample (Choi et al., 2017). When the stress reaches the maximum value of the whole curve, the corresponding strain is the failure strain (Fang et al., 2020). The ratio of unconfined compressive strength to failure strain is the elastic modulus (Li et al., 2016). In the first half of the stress–strain curve, the ratio of the stress at 50% of the failure strain to 50% of the failure strain is denoted as the elastic modulus at 50% of the unconfined compressive strength (Li et al., 2016). The stress–strain curve enters the second half after failure strain. The stress decreases gradually and then enters the phase of relatively stable residual strength. Here, we take the stress at 10% strain as the residual strength (Li et al., 2016; Lv et al., 2021).

2.4.2 Determination of calcium carbonate content

The calcium carbonate content in the samples was determined by the pickling method. Specifically, the samples and fragments of samples were weighed and soaked in 2 mol/L hydrochloric acid solution until there were no bubbles in the solution (Al Qabany and Soga, 2013; Zhao et al., 2020b). At this

TABLE 2 Setting of working conditions of sand samples.

Test code	ET-0	ET-1-10	ET-2-10	ET-3-10	ET-4-10	ET-2-5	ET-2-15	ET-2-20
Fiber type	No fiber	Sisal fiber						
Fiber content/%	0	0.1	0.2	0.1	0.1	0.2	0.2	0.2
Fiber length/mm	0	10	10	10	10	5	15	20
Treatment times	3	3	3	3	3	3	3	3
UCS test times	3	3	3	3	3	3	3	3
SEM & XRD test	√	—	√	—	√	—	—	√
Wet-Dry cycle times	0,1,2,3,4,5	0	0,1,2,3,4,5	0	0	0	0	0

point, the calcium carbonate in the sample was completely dissolved. The solution was drained, and the sample was carefully rinsed with deionized water. The content of calcium carbonate (C_{CC})was obtained by weighing again after the sample was dry, as shown in Eq. 1.

$$C_{CC} = \frac{m_2 - m_1}{m_1} \qquad (1)$$

In the above formula, m_1 is the mass after pickling and drying, and m_2 is the mass before pickling. Approximately 20 g of sample in the corresponding position was taken for the pickling test to calculate the calcium carbonate content of the top, middle and bottom of the sample. A pickling test was carried out on the whole sample when calculating the whole calcium carbonate content.

2.4.3 Solution analysis

1) Effect of materials on urease solution activity: The urease solution volume was 40 ml. Sand particles and sisal fibers were directly added into the urease solution. The mass of the sand particles (S1) and sisal fibers (S2) was 0.2% of the urease solution (Yuan et al., 2022). Urease solution without other materials was used as the control (S0). The change in urease activity with time was measured at 50°C, which is the temperature that the sample is curing.
2) Change of urease activity in effluent over time: The effluent was monitored, and the urease activity was determined. The changes in urease activity in the effluent were recorded over time after infusion, including sand without fiber (E0) and sand column reinforced with 0.2% sisal fibers (E1).
3) The change in urease solution content over time: In this test, the quality of effluent was monitored. The amount of solution retained in the sample was calculated after the urease solution was injected. The urease adsorption capacity of the sand column over time was recorded after the urease solution was injected, including sand without fiber (R0) and sand

column reinforced with 0.2% sisal fibers (R1). The urease adsorption capacity was recorded as the mass ratio, that is, the ratio of the retention mass of the urease solution to the mass of the sample.
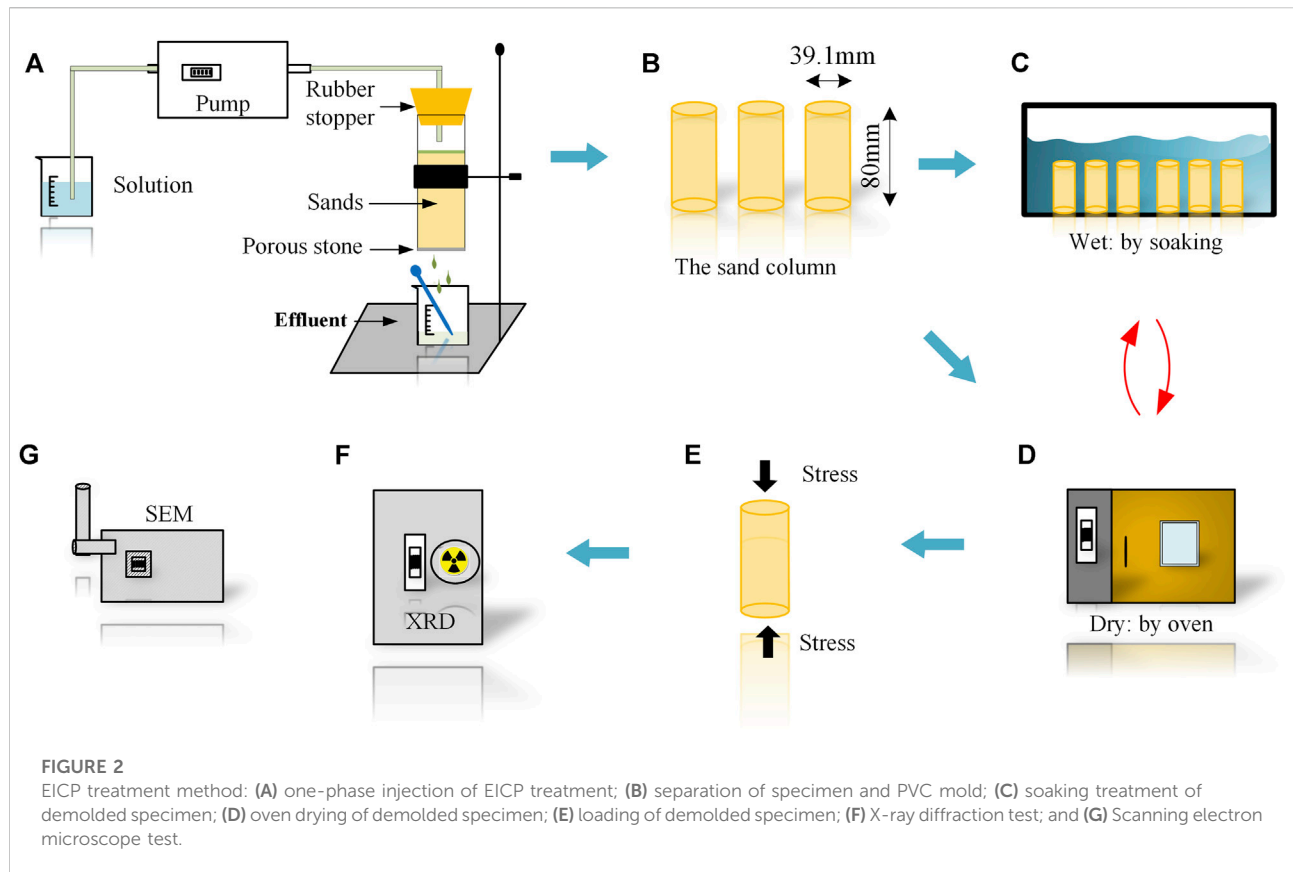
2.4.4 Microscopy

Portions of the sample and fibers were taken for SEM and X-ray diffraction analysis after EICP treatment. EICP-treated sand samples were imaged by a scanning electron microscope (FEI Quanta 250). Dry sand samples were selected for the test. Before SEM, the samples were flattened, and the loose soil particles were blown away manually with a stream of air from a rubber bulb. Then, each sample was glued to conductive paper and sprayed with gold before scanning. An X-ray diffraction analyser (D8-Advance) was used for crystal analysis of the EICP-treated sand. The test process is shown in Figure 2.

3 Results

In this part, the urease activity and urease activity per unit mass were measured. The optimal concentration of soybean powder was selected for EICP treatment. Then, the effect of sisal fiber on treatment effect of EICP-treated sand was investigated. Choose the best fiber length and fiber content to study the degradation effect of wet-dry cycle on the sample.

## 3.1 Urease activity analysis

Urease activity is one of the key factors affecting EICP treatment (Almajed, 2017). It reflects the hydrolysis rate of urea by urease solution (Cui et al., 2017). Urease activity per unit mass is the ratio of urease activity to the mass of soybean power. At present, there is no unified standard for the selection of soybean power. Figure 3 shows the influence of soybean powder

FIGURE 2
EICP treatment method: **(A)** one-phase injection of EICP treatment; **(B)** separation of specimen and PVC mold; **(C)** soaking treatment of demolded specimen; **(D)** oven drying of demolded specimen; **(E)** loading of demolded specimen; **(F)** X-ray diffraction test; and **(G)** Scanning electron microscope test.

concentration on urease activity and urease activity per unit mass. With the increase of soybean powder concentration, urease activity increased gradually and showed an approximate linear increase trend. With the increase of soybean powder concentration, urease activity per unit mass decreased step by step. When the concentration of soybean powder was less than 40 g/L, the urease activity per unit weight decreased rapidly with the increase of the concentration of soybean powder. When the concentration of soybean powder increased from 40 g/L to 100 g/L, the urease activity per unit mass was relatively stable, showing a "plateau". When the concentration of soybean powder was more than 100 g/L, the urease activity per unit mass began to decrease again. The higher the concentration of soybean powder was, the more urease was extracted from the solution under the same conditions (Hamdan et al., 2013; Wu L. et al., 2021). Therefore, with the increase of soybean powder concentration, urease activity also gradually increased. The higher the concentration of soybean powder, the lower the efficiency of urease extraction because of the limited solubility of aqueous solution (Blakeley and Zerner, 1983). Therefore, the urease activity per unit mass decreased with the increase of soybean powder concentration. When the soybean powder concentration was less than 40 g/L, the urease extraction efficiency was high, but the urease activity was low. When the concentration of soybean

FIGURE 3
Effect of soybean powder concentration on urease activity.
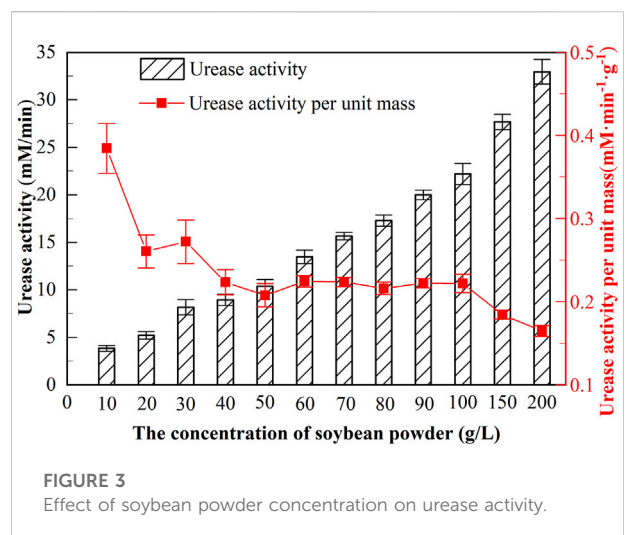
powder was between 40 g/L and 100 g/L, the urease activity per unit mass was relatively stable, indicating that the urease extraction efficiency was similar. In this range, the highest urease activity was 22.496 mM/min when the soybean powder concentration was 100 g/L. Therefore, 100 g/L was selected as soybean powder concentration.

FIGURE 4
Typical stress-strain curves.
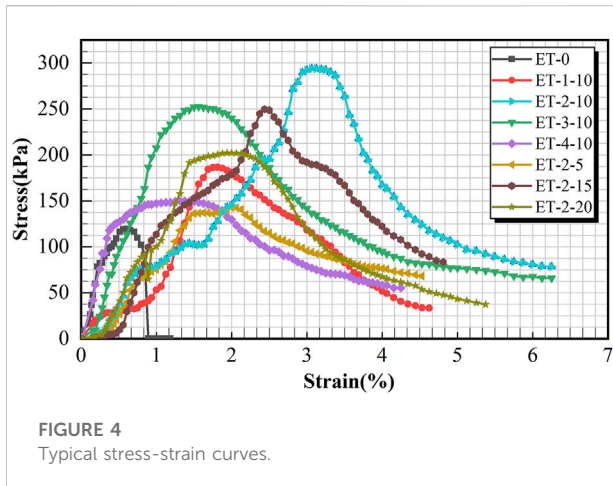
3.2 Typical stress-strain curves

The unconfined compressive strength test was conducted, and the typical stress-strain curves obtained were shown in Figure 4. It can be seen that the stress and strain characteristics of EICP-treated sand are obviously different after adding sisal fibers. Under the action of axial stress, the stress-strain curve of EICP-treated sand without fiber can be divided into two stages: with the increase of strain, the stress of the sample gradually increases. This is the first stage. Subsequently, the stress of the sample decreases suddenly. This is the second stage. The strain of the sample is less than 1% from the beginning of the destruction to the complete destruction. The variation characteristics of these two stages indicate that the failure of EICP-treated sand without fiber is typical brittle failure (Choi et al., 2016; Zhao et al., 2020a). When the unconfined compressive strength test is carried out on the samples with different fiber content and fiber length, the samples undergo three stages: in the first stage, the stress of the samples increases with the increase of strain; When the stress reaches the maximum value, the specimen is destroyed, and the stress-strain curve has an inflection point, The stress begins to change from increasing to decreasing, which is the second stage. In the third stage, the stress decreases with the increase of strain and eventually tends to be relatively stable. The specimen exhibits toughness (Fang et al., 2020; Lv et al., 2021). This feature was also observed by Li (Li et al., 2016) and Xiao (Xiao et al., 2019).

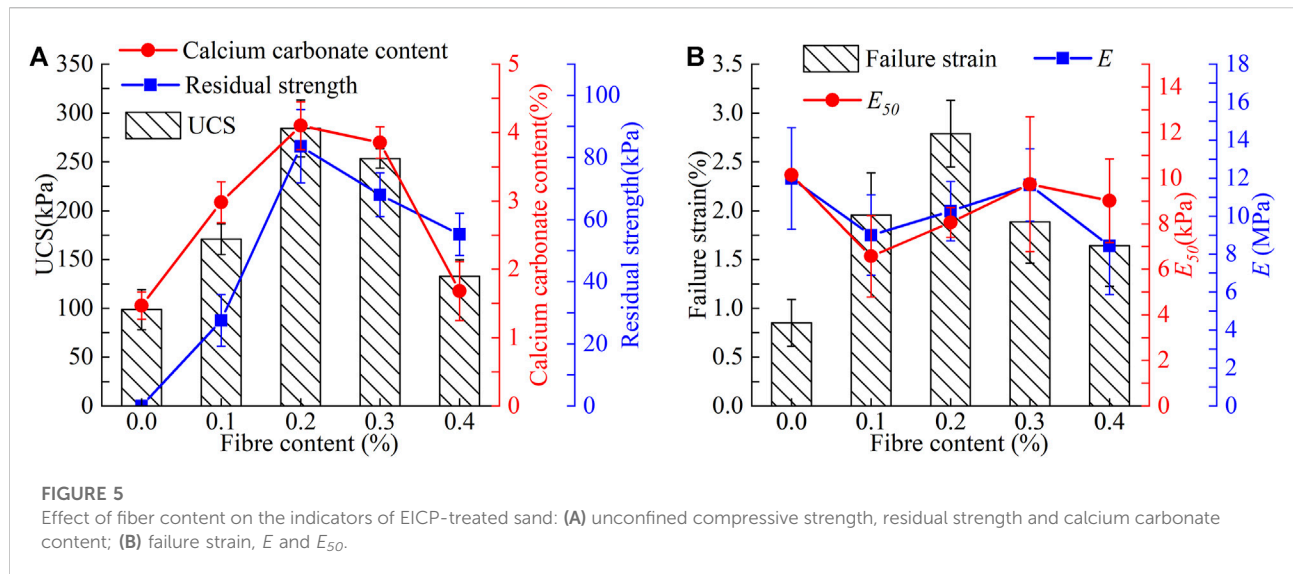## 3.3 Effect of fiber content on enzyme-induced calcium carbonate precipitation-treated sand

The effect of fiber content on unconfined compressive strength (UCS) is shown in Figure 5A. With the increase of fiber content, the UCS increases first and then decreases. The maximum UCS occurs at a fiber content of 0.2%. The UCS of the sample reached 293.8 kPa, which was 288% of that of the sample without fiber (98.62 kPa). When the fiber content is low, with the increase of fiber content, the effect of fiber in the sample changes from weak to strong. This limits the displacement and dislocation of each part in the sample. The UCS of the sample increases with the increase of fiber content in the initial stage (Almajed et al., 2018; Zhao et al., 2020b; Tang et al., 2020). However, when the fiber content is too high, aggregation will lead to uneven cementation (Yao et al., 2021). This reduces the bearing capacity of the sample.

It is generally believed that one of the important indexes to evaluate the effect of EICP treatment on sand is calcium carbonate content (C_{CC}). The C_{CC} increases first and then decreases with the increase of fiber content. The C_{CC} of EICP-treated sand without fiber was the lowest, which is 1.47%. The C_{CC} reached 4.1% when the fiber content was 0.2%. The smooth surface of quartz sand is not conducive to the adsorption of urease solution, which is a common problem in EICP treatment (Almajed, 2017; Cui et al., 2017; Arab et al., 2021). After sisal fiber was added, the internal specific surface area of the sample increased, and the retention ability of urease and cementing solution was enhanced (Phillips et al., 2013). This will effectively reduce the loss of solution during the grouting process. The C_{CC} is thus increased (the rough surface of sisal fiber is shown in Figure 1E). Fibers increase the urease "colonization domain" (Wen et al., 2018). When urease solution enters the soil, there are more favorable adsorption areas. Thus, it is beneficial to the formation and development of calcium carbonate crystal. But the internal pore volume of soil is constant. Due to the low density of fibers, the pore space will be compressed when there are too many fibers, and the capacity of soil to the solution will be reduced (Zhan et al., 2016).

Residual strength is an indicator of a material's toughness (Kiran and Ramakrishna, 2019). The greater the residual strength, the stronger the continuous bearing capacity of the material (Castoldi et al., 2019; Sharma et al., 2019). Materials with brittle failure often have no residual strength (Spencer and Sass, 2019). The residual strength increases first and then decreases with the increase of fiber content. The maximum value appeared when the fiber content was 0.2% and the fiber length was 10 mm. When the specimen reaches the peak compressive strength, the fiber can limit the development of cracks and delay the overall failure of the specimen (Lv et al., 2021). The limiting effect of fibers is related to the number of fibers in the fracture section (Yao et al., 2021). The more fibers, the more limiting the effect. However, too much fibers cannot effectively limit the crack progression (Choi et al., 2019). That will not be conducive to the continuous loading of samples due to agglomeration.

Similar to the variation of unconfined compressive strength (UCS), the failure strain of the sample increases first and then decreases with the increase of fiber content (Figure 5B). The peak point of failure strain coincides with the UCS when the fiber

FIGURE 5
Effect of fiber content on the indicators of EICP-treated sand: **(A)** unconfined compressive strength, residual strength and calcium carbonate content; **(B)** failure strain, E and E_{50}.
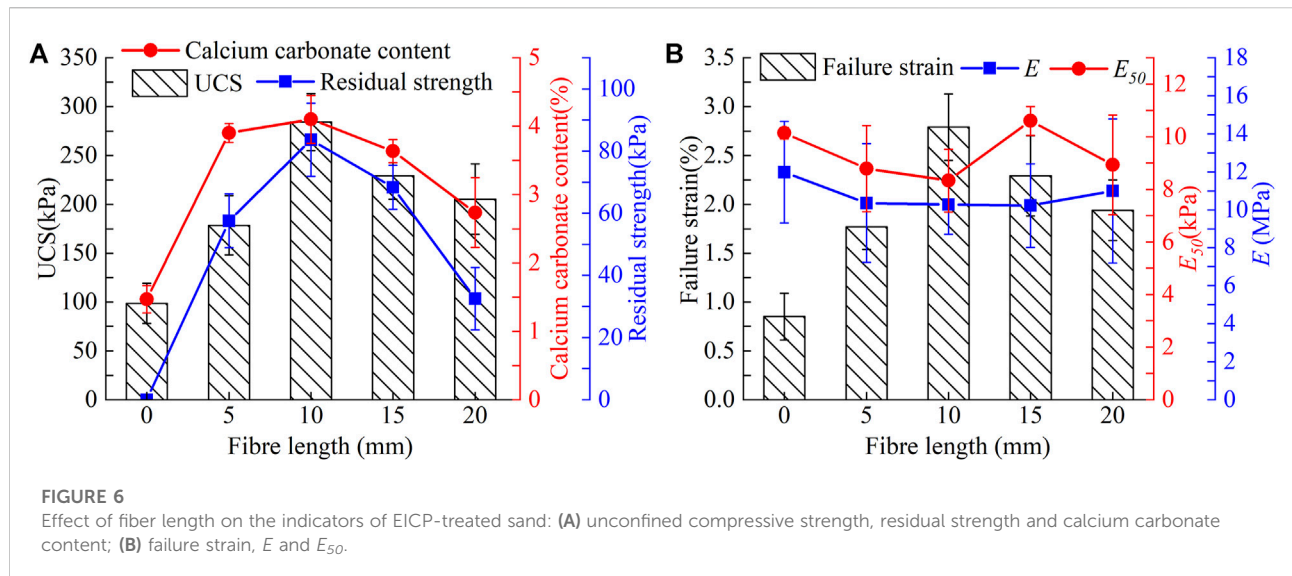
content is 0.2%. At this time, the failure strain reaches 2.8%, which is 3.29 times that of the failure strain without fiber. It can be seen that adding proper content of fibers can significantly improve the toughness of EICP-treated sand (Li et al., 2016). The fiber can limit the deformation of the samples. The sample containing fiber can bear higher stress under the same strain. When the fiber content is too high, the fiber agglomeration is serious and the resistance to deformation of the sample decreases (Zhao et al., 2020b). The specimen will fail rapidly, so the failure strain will be smaller.

In order to further analyze the toughness improvement of sisal fiber on the sample, elastic modulus (E) and elastic modulus at 50% of the unconfined compressive strength (E_{50}) were selected for analysis (Figure 5B). It can be seen that the E of specimens decreases after sisal fiber is added. The value of elastic modulus depends on peak strength and failure strain. It is proportional to peak stress and inversely proportional to failure. As shown in Figure 5A, the strength of sisal fiber sample was greatly improved. However, at the same time, the failure strain of the sample increases greatly. In general, the E and E_{50} of the specimen is smaller both before and during the whole stage. In the stress-strain diagram, the peak stress point moves to the upper right. This pattern is typical of the action of fibers (Li et al., 2016). That is, the strength increases with the expansion of strain range. This is an increase in toughness (Li et al., 2016; Al-Salloum et al., 2017; Xiao et al., 2019). The strength change caused by the increase of calcium carbonate content is different from this improvement effect of fiber. The increase in calcium carbonate content will cause the peak stress moving to the upper right and left on the stress-strain curve (Xiao et al., 2019). This increase in strength results in a narrowing of the strain range, which is brittle (Xiao et al., 2019).

3.4 Effect of fiber length on enzyme-induced calcium carbonate precipitation-treated sand

Fiber length is another important factor affecting the mechanical properties of EICP-treated sand (Fang et al., 2020). The unconfined compressive strength (UCS) of the sample increases first and then decreases with the increase of fiber length (Figure 6A). The maximum UCS occurs when the fiber length is 10 mm. The longer the fiber is, the more sand particles can be connected when the fiber is in a certain length range (De Melo et al., 2019). The anchorage range and effect increase with the increase of fiber length, and the increase of anchorage effect will lead to the increase of macroscopic strength (Jiang et al., 2021). But when fiber is too long, the long fibers tend to bend and eventually accumulate in sand. This reduces the efficiency of fiber action, resulting in a decline in UCS. When the sample reaches the peak strength, cracks often develop along the weak part (Larsen et al., 2008a). The fibers limit this, and the residual deformation stage. This limitation is not only related to fiber content, but also to fiber length. The longer the fiber length, the longer the anchorage length. The stronger the anchorage, the greater the overall residual stress. The effects of bending and agglomeration on residual strength are similar for overlong fibers. The influence of fiber length on calcium carbonate content (C_{CC}) is shown in Figure 6A. C_{CC} increased first and then decreased with the increase of sisal fiber length. The effect of fiber length on C_{CC} also increased first and then decreased. The peak value is reached when the fiber length is 10 mm. Too long fibers are unable to stretch to absorb more urease efficiently due to folding and aggregation (Phillips et al., 2013). It also reduces the C_{CC}.

The failure strain increases first and then decreases with the increase of fiber length (Figure 6B). The maximum failure strain is obtained when the fiber length is 10 mm. When subjected to the

FIGURE 6
Effect of fiber length on the indicators of EICP-treated sand: **(A)** unconfined compressive strength, residual strength and calcium carbonate content; **(B)** failure strain, E and E_{50}.

same amount of stress, longer fibers can lose load-bearing properties in some areas and still have effective resistance to external forces and deformation. Too long fibers can be bent. The elastic modulus (E) and elastic modulus at 50% of the unconfined compressive strength (E_{50}) of EICP-treated sand reinforced with different fiber length is also smaller than that without fiber. This mechanism is the same as in the analysis of fiber content. Too short and too long fibers cannot increase the deformation of samples.

## 3.5 Effects of wet-dry cycles

Natural fibers are almost always biodegradable (Kiran and Ramakrishna, 2019), which means they are unstable in their natural state (Liu et al., 2021). Among all the environmental factors, the wet-dry cycles is the most critical factor that degrades the structure and mechanical properties of natural fibers (Senthilkumar et al., 2018). Therefore, it is necessary to investigate the strength change of sisal fiber reinforced sand treated by EICP under the wet-dry cycles. The strength of sand with 10 mm length and 0.2% sisal fiber (optimal fiber parameter) treated by EICP was investigated after the wet-dry cycles. Sand treated with EICP without fiber was used as control. Figure 7 shows the influence of wet-dry cycles on unconfined compressive strength and mass loss of samples. The unconfined compressive strength of EICP treated sand and EICP treated sisal fiber reinforced sand decreased with the increase of wet-dry cycles times. The mass loss increases with the increase of wet-dry times. The unconfined compressive strength decreases the most during the first wet-dry cycle. Similar phenomena have been observed in previous studies (Cheng et al., 2017; Liu et al., 2019). The unconfined compressive strength decreases with the decrease of wet-dry cycles after 3 times. The unconfined compressive strength of EICP-treated sand and

FIGURE 7
Effect of wet-dry cycles on unconfined compressive strength, mass loss and strength loss ratio.
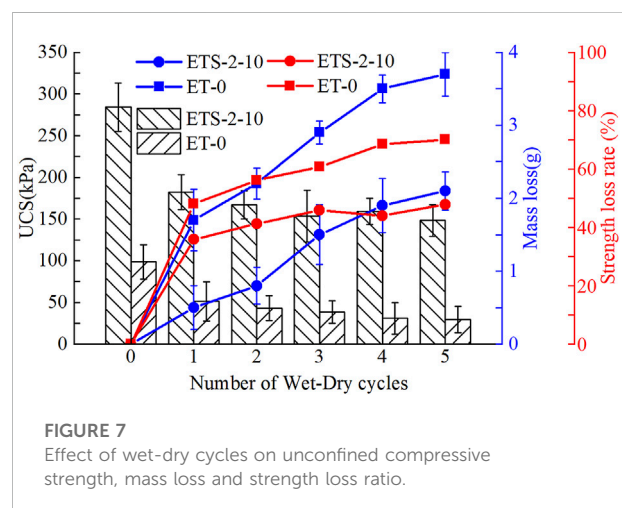
EICP-treated sisal fiber reinforced sand decreased to 148.3 and 29.5 kPa, respectively. The mass loss of EICP-treated sand and sisal fiber reinforced sand was 1.9 and 3.18 g, respectively, compared with the sand without wet-dry cycles. Compared with the strength loss ratio of 70.09%, the strength loss ratio of 0.2% sisal fiber sand treated by EICP was only 47.83% after five cycles of wet-dry. The durability of EICP-treated sand reinforced with sisal fiber is better under wet-dry cycles.

4 Discussion

In this part, the failure state and microstructure of specimens before and after adding sisal fibers were analyzed in order to explore the role of fibers. Further, more detailed microstructures of each sample were analyzed. As a supplement to the
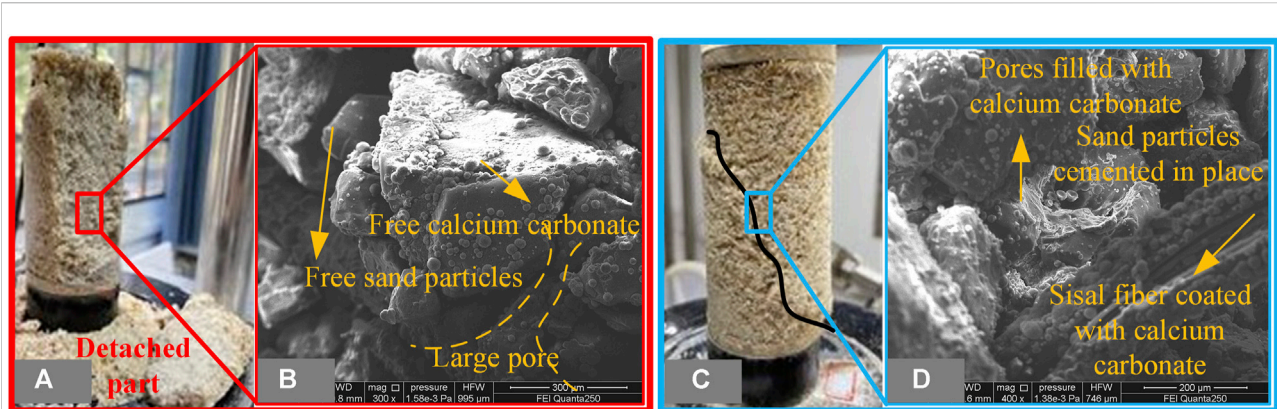
FIGURE 8
Failure crack of EICP-treated sand without fiber: **(A)** macroscopic image; **(B)** microscopic images. Failure crack of EICP-treated sand reinforced with sisal fibers: **(C)** macroscopic image; **(D)** microscopic images.

microscopic conclusions, the effect of calcium carbonate on strength was quantitatively analyzed. The results of solution analysis were used as a reference. The crystal form of calcium carbonate is also studied. Finally, the mechanism of sisal fiber is summarized.

4.1 Failure crack analysis

The strength and toughness of sisal fiber reinforced sand can be improved not only by mechanical index analysis. The failure patten of specimens can also be used as an intuitive representation of ductility and brittleness (Pooni et al., 2021). At the same time, it can also provide a basis for analyzing the changes of mechanical indexes of samples. The failure state is only related to the uniformity of cementation. The failure patten of samples were obviously different after the sisal fiber was added, as shown in Figure 8. The brittle failure of EICP-treated sand without fiber is caused by external force. Cracks first appear along the weak surface of the sample. With further loading, the weak surface of the sample was rapidly transfixed (Figure 8A). There is no constraint to stop this process. The sample is partially detached. At this point, the axial stress of the sample will suddenly drop to 0 (Li et al., 2016; Almajed, 2017; Lv et al., 2021). Unlike EICP-treated sand without fiber, EICP-treated sand reinforced with sisal fibers did not fall off in large chunks (Figure 8C), which meant that the specimens had a wider range of residual deformation and could continue to bear loads. This is mainly due to the limitation of sisal fibers on the weak side of EICP-treated sand reinforced by sisal fibers (Minto et al., 2018).

Scanning electron microscopy (SEM) was performed on the failure surfaces of the above two samples (Figures 8B,D). It can be seen that in EICP-treated sand without fiber, calcium carbonate

is unevenly distributed, mainly located on sand particles (El Mountassir et al., 2018; Arab et al., 2021). A small amount of calcium carbonate crystals cannot wrap sand particles, nor can they effectively fill the pores of sand particles (Mujah et al., 2021). The fault of discrete sand particles and calcium carbonate crystals lies in the sand. After sisal fiber was added, the coverage of calcium carbonate was significantly stronger (Almajed et al., 2018). Calcium carbonate fills the pores of sand particles and wraps up the fibers. This results in stronger internal integrity of the sample. It will also lead to stronger mechanical properties and durability to wet-dry cycles.

4.2 Scanning electron microscope analysis

The above analysis shows that the failure modes and internal structures of the specimens are obviously different after fibers addition. Sisal fiber obviously optimized the structure of EICP-treated sand. In this part, the influence of fiber content and fiber length on the internal structure of EICP-treated sand will be studied in more detail. Scanning electron microscopy tests were carried out to observe the microstructure of different samples. A typical image is selected as shown in Figure 9.

The internal pores of soil without fiber are larger and the calcium carbonate is sparse. When the fiber length was 10mm, the fiber distribution of sisal fiber reinforced sand with 0.1% content was sparse after EICP treatment. At this point, the fibers cannot form a "bridge" (Xiao et al., 2019). When the fiber content is 0.2%, the fibers are in a network. Calcium carbonate fills the pores and binds the fibers to the sand particles. Fibers become good three-dimensional bridges. This is conducive to the loading state of the sample (Ibraim et al., 2012; Hao et al., 2018; Choi et al., 2019). At a fiber content of 0.3%, the fibers began to show slight aggregation. Calcium carbonate is not evenly and
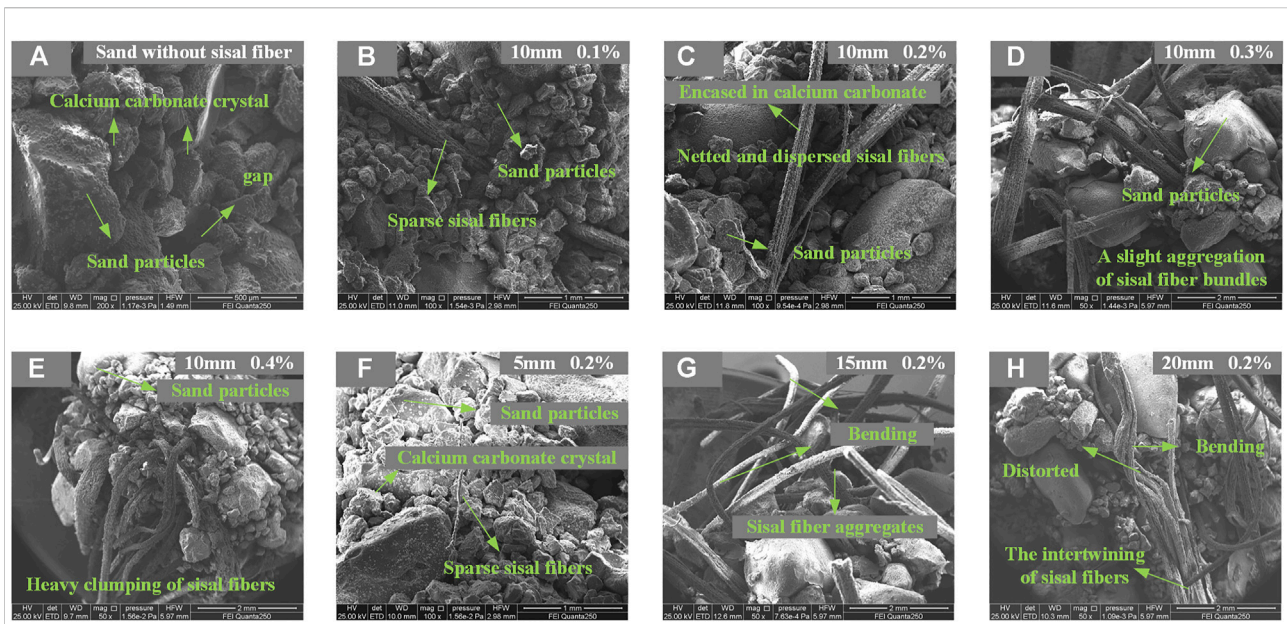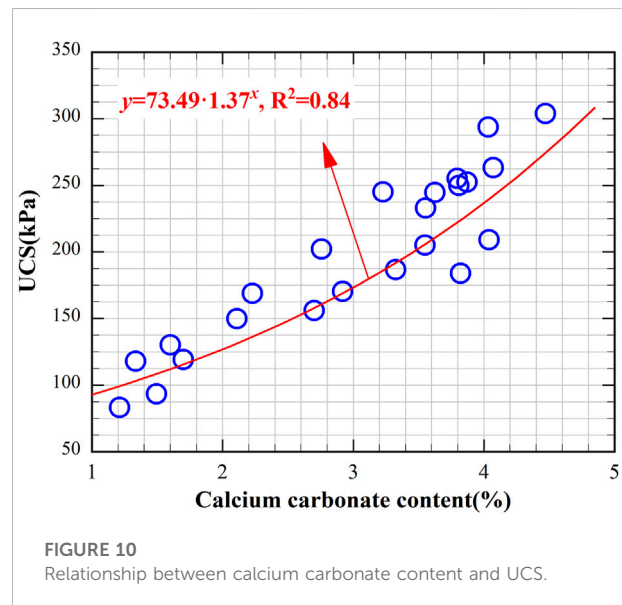
FIGURE 9
SEM images of EICP-treated sand reinforced with sisal fibers at different fiber contents: **(A)** 0%; **(B)** 0.1%; **(C)** 0.2%; **(D)** 0.3%; **(E)** 0.4%. SEM images of EICP-treated sand reinforced with sisal fibers at different fiber lengths: **(F)** 5 mm; **(G)** 15 mm; **(H)** 20 mm.

efficiently distributed around the aggregate. This will reduce the mechanical properties of samples to a certain extent (Ibraim et al., 2012; Li et al., 2016). As the fiber content increased to 0.4%, the agglomeration phenomenon became more obvious, and the particles around the large aggregates were loose (Yao et al., 2021). Calcium carbonate is produced less and the cementation effect is poor. When the fiber content is 0.2%, the fiber distribution of 5 mm longsword fiber is also more discrete. And a single short fiber cannot serve as a bridge (Xiao et al., 2019). The sisal fiber of 15 mm was bent in many parts of soil and aggregated to a certain extent. 20mm sisal fiber bending and aggregation phenomenon is more serious. If the distribution is too sparse or dense, and the bending phenomenon occurs, the cementing effect will be reduced (Hao et al., 2018).

4.3 Relationship between C_{CC} and unconfined compressive strength

The above analysis shows that calcium carbonate will be formed in the pores of sand particles after EICP treatment. In the presence of sisal fiber, calcium carbonate will also be generated in large quantities near sisal fiber. The calcium carbonate allows sisal fibers to connect effectively to the inner parts of the sand. It can also be seen from Figures 5, 6 that calcium carbonate content (C_{CC}) is positively correlated with sample strength. In order to confirm the influence of C_{CC} on the unconfined compressive strength (UCS) of samples, and further quantify the

FIGURE 10
Relationship between calcium carbonate content and UCS.

relationship. The relationship between UCS and C_{CC} was fitted, and the results were shown in Figure 10. It can be seen that in this experiment, C_{CC} was exponential with UCS. Compared with the previous experimental results, it is found that the fitting results are similar to those of soil without fiber (Choi et al., 2016; Cheng et al., 2017; Cui et al., 2017). For fiber-reinforced sand, C_{CC} is no longer the only factor determining the strength of EICP-treated sand (Fang et al., 2020). Fiber plays an
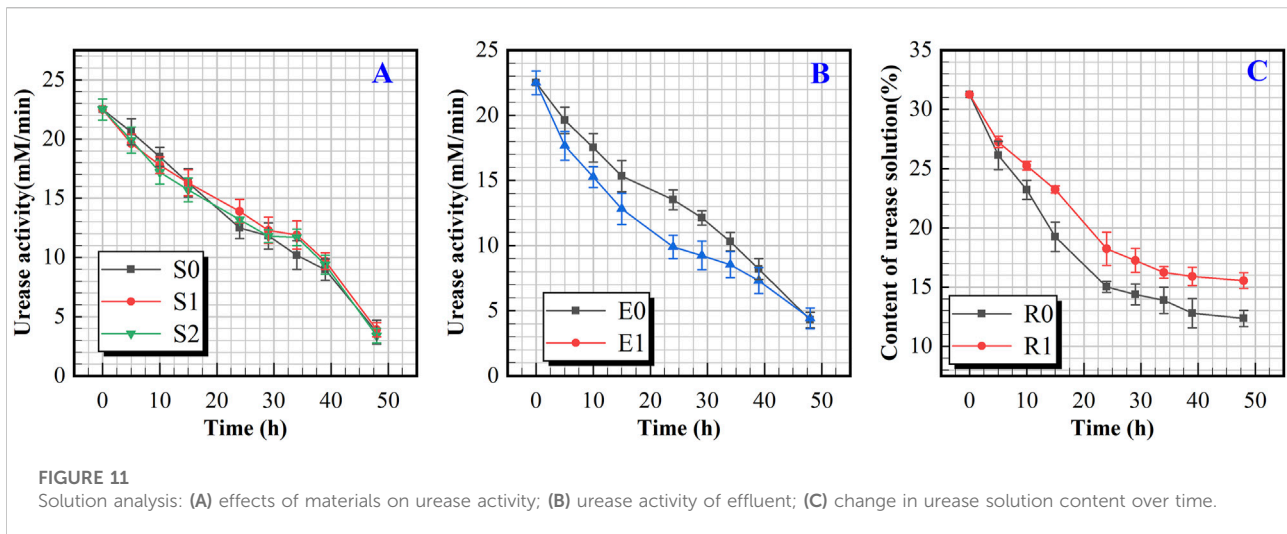
FIGURE 11
Solution analysis: **(A)** effects of materials on urease activity; **(B)** urease activity of effluent; **(C)** change in urease solution content over time.

equally important role as a bridge in soil. Fiber length, fiber content and fiber surface characteristics all affect the strength of the sample, and fiber can further improve the mechanical properties of the sample with calcium carbonate cementation (Hejazi et al., 2012).

4.4 Solution analysis

In order to support the above conclusion, the possibility of sand particles and sisal fiber participating in the reaction to reduce urease activity was excluded (Yuan et al., 2022). The urease activity of urease solution was compared with that of 0.2% sand particles and 0.2% sisal fibers. As shown in Figure 11A. The enzyme activities of the three solutions decreased with the increase of time, and the urease activities of the three solutions were less than 5% different. After 40h, the enzyme activities of the three solutions decreased rapidly to about 4 mM/ min. This indicated that sand particles and sisal fiber had little effect on urease activity (Almajed et al., 2018; Xiao et al., 2020; Yao et al., 2021).

Figure11B shows the changes of urease activity in effluent after drips of urease solution in sand without fiber and 0.2% sisal fiber sand. It can be seen that the urease activity of effluent decreased rapidly within 0–10 h. Within 20–40 h, the change is gentle, and then decreases rapidly after 40 h. The urease activity of leachate of sand with fiber addition was lower than that of sand without fiber addition, and the difference of urease activity also increased gradually. At 40 h, the urease activity of the effluent from the two samples was close again and decreased to about 4.3 mm/ min. At the beginning, the urease activity of leachate decreased rapidly due to the adsorption of urease by sand and fiber. When saturated by adsorption, the change of urease activity in leachate tended to be gentle. Urease could not be stored at room temperature

for a long time, and the urease activity of the whole solution would decrease after 40 h (Meng et al., 2021). At this point, the effect of fiber adsorption is no longer significant. Therefore, the urease activities in leachate of the two samples decreased significantly after 40 h. The adsorption capacity of sisal fiber to urease was greater than that of pure sand.

To explore the overall adsorption effect of sand with sisal fiber on urease solution. The urease solution content over time was compared between sand without fiber and 0.2% sisal fiber reinforced sand, as shown in Figure 11C. The urease solution
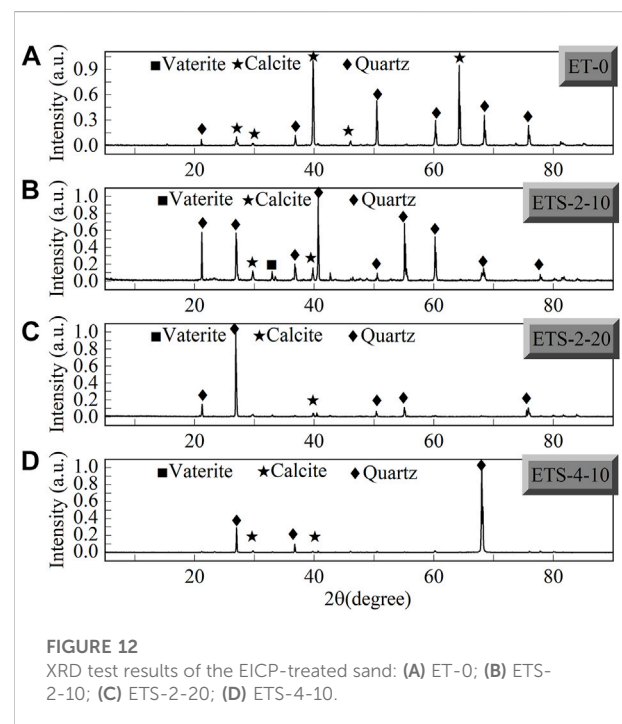

FIGURE 12
XRD test results of the EICP-treated sand: **(A)** ET-0; **(B)** ETS-2-10; **(C)** ETS-2-20; **(D)** ETS-4-10.

content in sand column decreases with time, and the decreasing speed gradually decreases. The adsorption effect of without fiber sand on urease solution was weaker than that of 0.2% sisal fiber reinforced sand. The adsorption capacity of urease solution remained relatively stable after 40 h. Fiber itself has little effect on urease activity, but fiber has strong adsorption effect on urease solution. It can maintain the high urea hydrolysis capacity in the sand for a long time, which is the reason why the calcium carbonate production in the fiber reinforced sand is higher than that in the unreinforced sand.
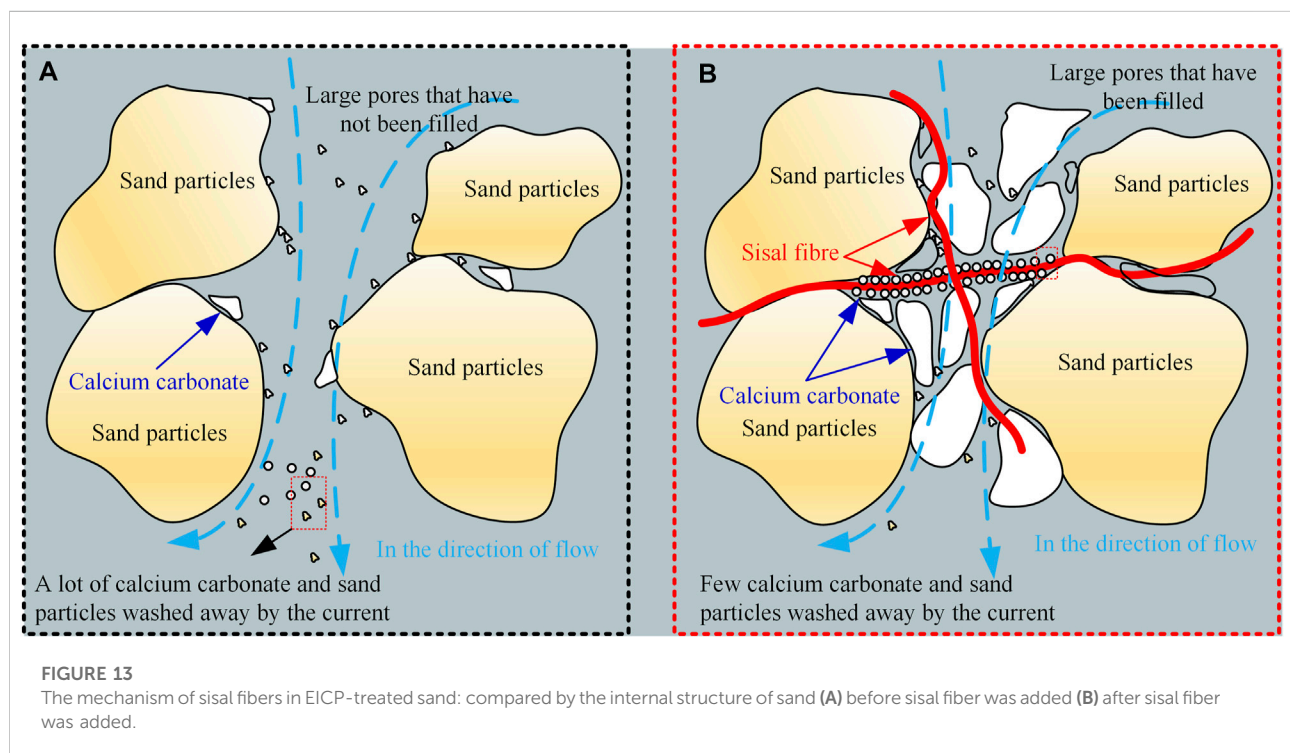
4.5 Crystal analysis

The above research confirms again that the improvement of mechanical properties of EICP-treated sand depends on the cementation of calcium carbonate. Without the cementation of calcium carbonate, the fibers would not be able to effectively connect the various parts of the sand (Neupane et al., 2013). However, studies have shown that the type of calcium carbonate crystal is affected by many factors such as temperature, urease concentration and fiber surface roughness (Almajed, 2017). In addition, the difference of fiber surface microstructure will lead to different precipitation patterns of calcium carbonate, resulting in different crystal types of calcium carbonate (Qiu et al., 2019). Different crystal types of calcium carbonate have significant influence on the mechanical properties of sand (Carmona et al., 2018). Calcium carbonate crystal types generally include calcite and

vaterite (Xiao et al., 2021). Vaterite is the crystal with the stronger cementation, but its physical and chemical properties are unstable (Zhao et al., 2020b). Studies have shown that vaterite may be converted to calcite when the ambient temperature is higher than 60°C (Xiao et al., 2018). This process is accompanied by a change in the properties of calcium carbonate (Phillips et al., 2013; Sun et al., 2021). Calcite can maintain strong cementation and have more stable physical and chemical properties (Yang et al., 2017). In this experiment, four typical samples were selected for XRD crystal analysis. Figure 12 shows the XRD images of each sample. It can be seen that the crystal type of calcium carbonate generated by soil in this study is mainly calcite with relatively stable properties. Vaterite existed in the group with the optimal mechanical properties (ETS-2–10), which has a stronger cementation. This may be the reason for the stronger mechanical properties of EICP-treated sand at this fiber parameter.

4.6 Summary of mechanism

Sisal fibers provide nucleation sites for calcium carbonate formation, which increased calcium carbonate conversion during EICP treatment (Figures 5, 6) (Almajed, 2017; Liu et al., 2019). This is mainly due to the rough surface area and large specific surface area of sisal fiber (Figure 1) (Senthilkumar et al., 2018; Sharma et al., 2019). Therefore, it has a stronger adsorption effect on the solution (Figure 11). More calcium carbonate fills the more pores of sand particles. While the reduction of pores can

FIGURE 13
The mechanism of sisal fibers in EICP-treated sand: compared by the internal structure of sand **(A)** before sisal fiber was added **(B)** after sisal fiber was added.

reduce the brittleness of EICP-treated sand (Figure 4) (Xiao et al., 2019). In addition, calcium carbonate immobilizes the fibers in the sand, forming a bridge (Figure 9). This further improves the mechanical properties of the sample (Li et al., 2016; Hamdan, 2019; Lv et al., 2021). The strength sisal fiber decreases rapidly under wet-dry cycles (Kiran and Ramakrishna, 2019). However, this study found that sisal fiber reinforced sand treated with EICP have better durability (Figure 7). The fine sand particles and calcium carbonate particles dispersed in the sample are carried away by water flow during the alternation of wet-dry cycles (Liu et al., 2019). At the same time, the water also destroys the cement between the calcium carbonate and the sand particles, which are tightly bound together (Cheng et al., 2017; Liu et al., 2019). Resulting in the loss of strength and mass. Sisal fibers can be greatly affected by the wet-dry cycles, but it was found in this experiment that the sisal fiber reinforced sand treated by EICP still maintained a high strength after the wet-dry cycles. The sample can resist wet-dry cycles to a certain extent. The fibers make EICP treatment produce stronger cementation (Figure 8). More calcium carbonate will fill more pores and reduce the erosion of water flow during the wet-dry cycle (Figure 9) (Liu et al., 2019). Calcium carbonate can wrap and protect sisal fiber and weaken the effect of wet-dry cycles on sisal fiber itself. After EICP treatment, sisal fibers are tightly wrapped with calcium carbonate, which is insoluble in water and can protect fibers (Figure 8). The bridge function of fiber is not the only factor to improve the strength of EICP treated sand (Xiao et al., 2019; Lv et al., 2021). The increase of calcium carbonate content caused by fiber is also the factor to improve the strength of EICP-treated sand (Xiao et al., 2019). Therefore, the strength of EICP-treated samples can only be affected to a certain extent by the change of fiber properties under the action of wet-dry cycles. The mechanism summarized above is shown in Figure 13.

5 Conclusion

Sisal fiber reinforced sand was treated by EICP in this experiment. The effect of fiber content (0.1%, 0.2%, 0.3%, 0.4%) and fiber length (5, 10, 15, 20 mm) on EICP treatment was investigated. In view of the concern of wet-dry cycles on natural fibers, tests were carried out to explore the deterioration of samples after wet-dry cycles. Explore the mechanism in combination with microscopic experiments and solution analysis. The main conclusions are as follows:

1. Sisal fibers can improve the mechanical properties of EICP-treated sand effectively. The failure mode of the samples changed from brittle failure to ductile failure after fibers were added. When the fiber length was 10 mm and the fiber content was 0.2%, the mechanical properties improved most significant. At this time, the unconfined compressive strength, calcium carbonate content, failure strain and residual strength of EICP-treated sand are significantly improved. At the same time, E and E_{50} decreased to some extent.

2. Microscopic test results show that sisal fiber plays a "bridge" role in EICP-treated sand. Too few or too short fibers cannot form an effective "bridge" inside the sample. Too many fibers tend to clump together, while too long will be bend. These phenomena are not conducive to the mechanical properties of the sample and the formation of calcium carbonate. There are optimal parameters for fiber properties. In addition, under the optimal sisal fiber parameters, the sample generates a crystal form of calcium carbonate with stronger cementation (vaterite).

3. Sisal fiber has rough surface, large specific surface area and strong adsorption capacity for solution. That provide nucleation sites for calcium carbonate and increase the production amount of calcium carbonate. This results in stronger cementation. Meanwhile, more calcium carbonate fills more pores. This improves the mechanical properties of the samples and reduces the erosion of water flow during the wet-dry cycles. Calcium carbonate can wrap and protect sisal fiber, and weaken the effect of wet-dry cycles on sisal fiber. EICP-treated sand reinforced by sisal fiber can resist the wet-dry cycle better.

Data availability statement

The original contributions presented in the study are included in the article/Supplementary Material, further inquiries can be directed to the corresponding author.

Author contributions

Methodology and funding acquisition: JZ. Software: YY. Data curation and formal analysis: LS and HB. Visualization: WS. All authors have read and agreed to the published version of the manuscript.

Funding

Conflict of interest

The authors declare that the research was conducted in the absence of any commercial or financial relationships that could be construed as a potential conflict of interest.

Publisher's note

All claims expressed in this article are solely those of the authors and do not necessarily represent those of their affiliated organizations, or those of the publisher, the editors and the reviewers. Any product that may be evaluated in this article, or claim that may be made by its manufacturer, is not guaranteed or endorsed by the publisher.

References

Al Qabany, A., and Soga, K. (2013). Effect of chemical treatment used in MICP on engineering properties of cemented soils. *Geotechnique* 63, 331–339. doi:10.1680/geot.SIP13.P.022

Al-Salloum, Y., Hadi, S., Abbas, H., Almusallam, T., and Moslem, M. A. (2017). Bio-induction and bioremediation of cementitious composites using microbial mineral precipitation – a review. *Constr. Build. Mat.* 154, 857–876. doi:10.1016/j.conbuildmat.2017.07.203

Allen, S. K., Zhang, G., Wang, W., Yao, T., and Bolch, T. (2019). Potentially dangerous glacial lakes across the Tibetan Plateau revealed using a large-scale automated assessment approach. *Sci. Bull. (Beijing).* 64, 435–445. doi:10.1016/j.scib.2019.03.011

Almajed, A. (2017). Enzyme induced carbonate precipitation (EICP) for soil improvement. *Dr. deseration* 4.

Almajed, A., Khodadadi, H., and Kavazanjian, E. (2018). "Sisal fiber reinforcement of EICP-treated soil," in IFCEE 2018, Orlando, FL, March 5–10, 2018, 29–36. doi:10.1061/9780784481592.004

Arab, M. G., Rohy, H., Zeiada, W., Almajed, A., and Omar, M. (2021). One-phase EICP biotreatment of sand exposed to various environmental conditions. *J. Mat. Civ. Eng.* 33, 04020489. doi:10.1061/(asce)mt.1943-5533.0003596

ASTM D2166 (2013). *Standard test method for unconfined compressive strength of cohesive soil.* West Conshohocken: ASTM.

Blakeley, R. L., and Zerner, B. (1983). Jack bean urease: The first nickel enzyme. *Inorganica Chim. Acta* 79, 11. doi:10.1016/s0020-1693(00)95029-1

Carmona, J. P. S. D. F., Oliveira, P. J. V., Lemos, L., and Pedro, A. M. G. (2018). Improvement of a sandy soil by enzymatic calcium carbonate precipitation. *Proc. Institution Civ. Eng. - Geotechnical Eng.* 171, 3–15. doi:10.1680/jgeen.16.00138

Castoldi, R. D. S., de Souza, L. M. S., and de Andrade Silva, F. (2019). Comparative study on the mechanical behavior and durability of polypropylene and sisal fiber reinforced concretes. *Constr. Build. Mat.* 211, 617–628. doi:10.1016/j.conbuildmat.2019.03.282

Cheng, L., Shahin, M. A., and Mujah, D. (2017). Influence of key environmental conditions on microbially induced cementation for soil stabilization. *J. Geotech. Geoenviron. Eng.* 143, 04016083. doi:10.1061/(asce)gt.1943-5606.0001586

Choi, S.-G., Hoang, T., Alleman, E. J., and Chu, J. (2019). Splitting tensile strength of fiber-reinforced and biocemented sand. *J. Mat. Civ. Eng.* 31, 06019007. doi:10.1061/(asce)mt.1943-5533.0002841

Choi, S.-G., Park, S.-S., Wu, S., and Chu, J. (2017). Methods for calcium carbonate content measurement of biocemented soils. *J. Mat. Civ. Eng.* 29, 06017015. doi:10.1061/(asce)mt.1943-5533.0002064

Choi, S. G., Wang, K., and Chu, J. (2016). Properties of biocemented, fiber reinforced sand. *Constr. Build. Mat.* 120, 623–629. doi:10.1016/j.conbuildmat.2016.05.124

Cui, M. J., Lai, H. J., Hoang, T., and Chu, J. (2021). One-phase-low-pH enzyme induced carbonate precipitation (EICP) method for soil improvement. *Acta Geotech.* 16, 481–489. doi:10.1007/s11440-020-01043-2

Cui, M. J., Zheng, J. J., Zhang, R. J., Lai, H. J., and Zhang, J. (2017). Influence of cementation level on the strength behaviour of bio-cemented sand. *Acta Geotech.* 12, 971–986. doi:10.1007/s11440-017-0574-9

De Castro, B. D., Fotouhi, M., Vieira, L. M. G., de Faria, P. E., and Campos Rubio, J. C. (2021). Mechanical behaviour of a green composite from biopolymers reinforced with sisal fibres. *J. Polym. Environ.* 29, 429–440. doi:10.1007/s10924-020-01875-9

De Melo, K. M., Dos Santos, T. F., Santos, C. M. D. S., Da Fonseca, R. T., De Lucena, N. D., De Medeiros, J. I., et al. (2019). Study of the reuse potential of the sisal fibers powder as a particulate material in polymer composites. *J. Mat. Res. Technol.* 8, 4019–4025. doi:10.1016/j.jmrt.2019.07.010

DeJong, J. T., Fritzges, M. B., and Nüsslein, K. (2006). Microbially induced cementation to control sand response to undrained shear. *J. Geotech. Geoenviron. Eng.* 132132, 138111–141392. doi:10.1061/(asce)1090-0241(2006)132:11(1381)

El Mountassir, G., Minto, J. M., van Paassen, L. A., Salifu, E., and Lunn, R. J. (2018). *Applications of microbial processes in geotechnical engineering.* 1st ed. Amsterdam: Elsevier. doi:10.1016/bs.aambs.2018.05.001

Fang, X., Yang, Y., Chen, Z., Liu, H., Xiao, Y., and Shen, C. (2020). Influence of fiber content and length on engineering properties of MICP-treated coral sand. *Geomicrobiol. J.* 37, 582–594. doi:10.1080/01490451.2020.1743392

Frazão, C., Barros, J., Toledo Filho, R., Ferreira, S., and Gonçalves, D. (2018). Development of sandwich panels combining sisal fiber-cement composites and fiber-reinforced lightweight concrete. *Cem. Concr. Compos.* 86, 206–223. doi:10.1016/j.cemconcomp.2017.11.008

Gao, Y., Tang, X., Chu, J., and He, J. (2019). Microbially induced calcite precipitation for seepage control in sandy soil. *Geomicrobiol. J.* 36, 366–375. doi:10.1080/01490451.2018.1556750

Hamdan, N. M. (2019). Applications of enzyme induced carbonate precipitation (EICP) for soil improvement. *J. Chem. Inf. Model.* 53, 1689–1699.

Hamdan, N., Kavazanjian, E., and O'Donnell, S. (2013). "Carbonate cementation via plant derived urease," in 18th International Conference on Soil Mechanics and Geotechnical Engineering: Challenges and Innovations in Geotechnics, ICSMGE 2013, Paris, France, September 2–5, 2013, 1–11.

Hao, Y., Cheng, L., Hao, H., and Shahin, M. A. (2018). Enhancing fiber/matrix bonding in polypropylene fiber reinforced cementitious composites by microbially induced calcite precipitation pre-treatment. *Cem. Concr. Compos.* 88, 1–7. doi:10.1016/j.cemconcomp.2018.01.001

Hejazi, S. M., Sheikhzadeh, M., Abtahi, S. M., and Zadhoush, A. (2012). A simple review of soil reinforcement by using natural and synthetic fibers. *Constr. Build. Mat.* 30, 100–116. doi:10.1016/j.conbuildmat.2011.11.045

Huang, M., Jiang, S., Xu, C., and Xu, D. (2020). A new theoretical settlement model for large step-tapered hollow piles based on disturbed state concept theory. *Comput. Geotech.* 124, 103626. doi:10.1016/j.compgeo.2020.103626

Iamchaturapatr, J., Piriyakul, K., and Petcherdchoo, A. (2022). Characteristics of sandy soil treated using EICP-based urease enzymatic acceleration method and natural hemp fibers. *Case Stud. Constr. Mater.* 16, e00871. doi:10.1016/j.cscm.2022.e00871

Ibraim, E., Diambra, A., Russell, A. R., and Muir Wood, D. (2012). Assessment of laboratory sample preparation for fibre reinforced sands. *Geotext. Geomembranes* 34, 69–79. doi:10.1016/j.geotexmem.2012.03.002

Jiang, N. J., Wang, Y. J., Chu, J., Kawasaki, S., Tang, C. S., Cheng, L., et al. (2021). Bio-mediated soil improvement: An introspection into processes, materials, characterization and applications. *Soil Use Manag.* 38, 68–93. doi:10.1111/sum.12736

Jiang, N., Tang, C., Yin, L., Xie, Y., and Shi, B. (2019). Applicability of microbial calcification method for sandy-slope surface erosion control. *J. Mat. Civ. Eng.* 31, 04019250. doi:10.1061/(asce)mt.1943-5533.0002897

Khodadadii, H., Javadi, N., Krishnan, V., Hamdan, N., and Kavazanjian, E. (2020). Crude urease extract for biocementation. *J. Mat. Civ. Eng.* 32, 04020374. doi:10.1061/(asce)mt.1943-5533.0003466

Kiran, S. P., and Ramakrishna, A. N. (2019). Degradation of modified sisal fiber buried in black cotton and litomargic soil. *Int. J. Recent Technol. Eng.* 7, 040030.

Ladd, E. S. (1989). Properties of rocks and soils. *Dev. Geotech. Eng.* 48, 75–173. doi:10.1016/B978-0-444-98950-5.50008-3

Larsen, J., Poulsen, M., Agerbaek, M., and Lundgaard, T. (2008a2008). Plugging of fractures in chalk reservoirs by enzyme-induced calcium carbonate precipitation. SPE production & operation. *SPE Prod. Operations* 23 (4), 478–483. doi:10.2118/108589-PA

Larsen, J., Poulsen, M., Agerbaek, M., and Lundgaard, T. (2008b). Plugging of fractures in chalk reservoirs by enzyme-induced calcium carbonate precipitation. *SPE Prod. Operations* 23, 478–483. doi:10.2118/108589-pa

Lei, X., Lin, S., Meng, Q., Liao, X., and Xu, J. (2020). Influence of different fiber types on properties of biocemented calcareous sand. *Arab. J. Geosci.* 13, 317. doi:10.1007/s12517-020-05309-7

Li, M., Li, L., Ogbonnaya, U., Wen, K., Tian, A., and Amini, F. (2016). Influence of fiber addition on mechanical properties of MICP-treated sand. *J. Mat. Civ. Eng.* 28, 04015166. doi:10.1061/(asce)mt.1943-5533.0001442

Liu, J., Wu, D., Wang, T., Ji, M., and Wang, X. (2021). Interannual variability of dust height and the dynamics of its formation over East Asia. *Sci. Total Environ.* 751, 142288. doi:10.1016/j.scitotenv.2020.142288

Liu, S., Wen, K., Armwood, C., Bu, C., Li, C., Amini, F., et al. (2019). Enhancement of MICP-treated sandy soils against environmental deterioration. *J. Mat. Civ. Eng.* 31, 04019294. doi:10.1061/(asce)mt.1943-5533.0002959

Lv, C., Zhu, C., Tang, C. S., Cheng, Q., Yin, L. Y., and Shi, B. (2021). Effect of fiber reinforcement on the mechanical behavior of bio-cemented sand. *Geosynth. Int.* 28, 195–205. doi:10.1680/jgein.20.00037

Meng, H., Shu, S., Gao, Y., Yan, B., and He, J. (2021). Multiple-phase enzyme-induced carbonate precipitation (EICP) method for soil improvement. *Eng. Geol.* 294, 106374. doi:10.1016/j.enggeo.2021.106374

Mert Tezer, M., and Başaran Bundur, Z. (2022). Use of natural minerals to immobilize bacterial cells for remediating cracks in cement-based materials. *J. Mat. Civ. Eng.* 34, 1–13. doi:10.1061/(asce)mt.1943-5533.0004098

Minto, J. M., Tan, Q., Lunn, R. J., El Mountassir, G., Guo, H., and Cheng, X. (2018). 'Microbial mortar'-restoration of degraded marble structures with microbially induced carbonate precipitation. *Constr. Build. Mat.* 180, 44–54. doi:10.1016/j.conbuildmat.2018.05.200

Morán, J. I., Alvarez, V. A., Cyras, V. P., and Vázquez, A. (2008). Extraction of cellulose and preparation of nanocellulose from sisal fibers. *Cellulose* 15, 149–159. doi:10.1007/s10570-007-9145-9

Mujah, D., Shahin, M. A., Cheng, L., and Karrech, A. (2021). Experimental and analytical study on geomechanical behavior of biocemented sand. *Int. J. Geomech.* 21, 0002105. doi:10.1061/(asce)gm.1943-5622.0002105

Neupane, D., Yasuhara, H., Kinoshita, N., and Unno, T. (2013). Applicability of enzymatic calcium carbonate precipitation as a soil-strengthening technique. *J. Geotech. Geoenviron. Eng.* 139, 2201–2211. doi:10.1061/(asce)gt.1943-5606.0000959

Pasillas, J. N., Khodadadi, H., Martin, K., Bandini, P., Newtson, C. M., and Kavazanjian, E. (2018). "Viscosity-enhanced EICP treatment of soil," in IFCEE 2018, Orlando, FL, March 5–10, 2018, 145–154. doi:10.1061/9780784481592.015

Phillips, A. J., Gerlach, R., Lauchnor, E., Mitchell, A. C., Cunningham, A. B., and Spangler, L. (2013). Engineered applications of ureolytic biomineralization: A review. *Biofouling* 29, 715–733. doi:10.1080/08927014.2013.796550

Pooni, J., Robert, D., Gunasekara, C., Giustozzi, F., and Setunge, S. (2021). Mechanism of enzyme stabilization for expansive soils using mechanical and microstructural investigation. *Int. J. Geomech.* 21, 12–31. doi:10.1061/(asce)gm.1943-5622.0002164

Qiu, R., Tong, H., Fang, X., Liao, Y., and Li, Y. (2019). Analysis of strength characteristics of carbon fiber–reinforced microbial solidified sand. *Adv. Mech. Eng.* 11, 168781401988442–168781401988447. doi:10.1177/1687814019884420

Senthilkumar, K., Saba, N., Rajini, N., Chandrasekar, M., Jawaid, M., Siengchin, S., et al. (2018). Mechanical properties evaluation of sisal fibre reinforced polymer composites: A review. *Constr. Build. Mat.* 174, 713–729. doi:10.1016/j.conbuildmat.2018.04.143

Sharma, A. K., Prasannan, S., and Kolathayar, S. (2019). "Comparative study of sisal and PVA fiber for soil improvement," in Eighth International Conference on Case Histories in Geotechnical Engineering, Geocongress 2019, Philadelphia, Pennsylvania, USA, 2019, 30. doi:10.1061/9780784482117.030

Song, D., Liu, X., Li, B., Zhang, J., and Bastos, J. J. V. (2021). Assessing the influence of a rapid water drawdown on the seismic response characteristics of a reservoir rock slope using time–frequency analysis. *Acta Geotech.* 16, 1281–1302. doi:10.1007/s11440-020-01094-5

Spencer, C. A., and Sass, H. (2019). Use of carrier materials to immobilise and supply cementation medium for microbially mediated self-healing of biocement. *IOP Conf. Ser. Mat. Sci. Eng.* 660, 012067. doi:10.1088/1757-899X/660/1/012067

Sun, X., Miao, L., and Wu, L. (2020). Applicability and theoretical calculation of enzymatic calcium carbonate precipitation for sand improvement. *Geomicrobiol. J.* 37, 389–399. doi:10.1080/01490451.2019.1710625

Sun, X., Miao, L., Yuan, J., Wang, H., and Wu, L. (2021). Application of enzymatic calcification for dust control and rainfall erosion resistance improvement. *Sci. Total Environ.* 759, 143468. doi:10.1016/j.scitotenv.2020.143468

Tang, C. S., Yin, L. y., Jiang, N. j., Zhu, C., Zeng, H., Li, H., et al. (2020). Factors affecting the performance of microbial-induced carbonate precipitation (MICP) treated soil: A review. *Environ. Earth Sci.* 79, 94. doi:10.1007/s12665-020-8840-9

Wang, C., Liu, X., Song, D., Wang, E., and Zhang, J. (2021). Numerical investigation on dynamic response and failure modes of rock slopes with weak interlayers using continuum-discontinuum element method. *Front. Earth Sci.* 9, 1–15. doi:10.3389/feart.2021.791458

Wang, L., van Paassen, L., and Kavazanjian, E. J. (2020). Geo-congress 2020 GSP 317 612. *Geo-Congress 2020 GSP* 320 (1), 612–621.

Wen, K., Bu, C., Liu, S., Li, Y., and Li, L. (2018). Experimental investigation of flexure resistance performance of bio-beams reinforced with discrete randomly distributed fiber and bamboo. *Constr. Build. Mat.* 176, 241–249. doi:10.1016/j.conbuildmat.2018.05.032

Wu, L., Miao, L., Sun, X., and Wang, H. (2021). Enzyme-induced carbonate precipitation combined with polyvinyl alcohol to solidify aeolian sand. *J. Mat. Civ. Eng.* 33, 1–10. doi:10.1061/(asce)mt.1943-5533.0004009

Wu, S., Li, B., and Chu, J. (2021). Stress-dilatancy behavior of MICP-treated sand. *Int. J. Geomech.* 21, 04020264. doi:10.1061/(asce)gm.1943-5622.0001923

Xiao, P., Liu, H., Xiao, Y., Stuedlein, A. W., and Evans, T. M. (2018). Liquefaction resistance of bio-cemented calcareous sand. *Soil Dyn. Earthq. Eng.* 107, 9–19. doi:10.1016/j.soildyn.2018.01.008

Xiao, Y., Chen, H., Stuedlein, A. W., Evans, T. M., Chu, J., Cheng, L., et al. (2020). Restraint of particle breakage by biotreatment method. *J. Geotech. Geoenviron. Eng.* 146, 04020123. doi:10.1061/(asce)gt.1943-5606.0002384

Xiao, Y., He, X., Evans, T. M., Stuedlein, A. W., and Liu, H. (2019). Unconfined compressive and splitting tensile strength of basalt fiber–reinforced biocemented sand. *J. Geotech. Geoenviron. Eng.* 145, 04019048. doi:10.1061/(asce)gt.1943-5606.0002108

Xiao, Y., Stuedlein, A. W., He, X., Han, F., Evans, T. M., Pan, Z., et al. (2021). Lateral responses of a model pile in biocemented sand. *Int. J. Geomech.* 21, 06021027. doi:10.1061/(asce)gm.1943-5622.0002179

Yang, P., O'Donnell, S., Hamdan, N., Kavazanjian, E., and Neithalath, N. (2017). 3D DEM simulations of drained triaxial compression of sand strengthened using microbially induced carbonate precipitation. *Int. J. Geomech.* 17, 04016143. doi:10.1061/(asce)gm.1943-5622.0000848

Yao, D., Wu, J., Wang, G., Wang, P., Zheng, J. J., Yan, J., et al. (2021). Effect of wool fiber addition on the reinforcement of loose sands by microbially induced carbonate precipitation (MICP): Mechanical property and underlying mechanism. *Acta Geotech.* 16, 1401–1416. doi:10.1007/s11440-020-01112-6

Yuan, H., Liu, K., Zhang, C., and Zhao, Z. (2022). Mechanical properties of Na-montmorillonite-modified EICP-treated silty sand. *Environ. Sci. Pollut. Res.* 29, 10332–10344. doi:10.1007/s11356-021-16442-5

Zhan, Q., Qian, C., and Yi, H. (2016). Microbial-induced mineralization and cementation of fugitive dust and engineering application. *Constr. Build. Mat.* 121, 437–444. doi:10.1016/j.conbuildmat.2016.06.016

Zhang, D., Sun, Z., and Fang, Q. (2022). Scientific problems and research proposals for Sichuan–Tibet railway tunnel construction. *Undergr. Space* 7, 419–439. doi:10.1016/j.undsp.2021.10.002

Zhang, J., Wang, X. J., Shi, L., and Yin, Y. (2022). Enzyme-induced carbonate precipitation (EICP) combined with lignin to solidify silt in the Yellow River flood area. *Constr. Build. Mat.* 339, 127792. doi:10.1016/j.conbuildmat.2022.127792

Zhao, Y., Fan, C., Ge, F., Cheng, X., and Liu, P. (2020a). Enhancing strength of MICP-treated sand with scrap of activated carbon-fiber felt. *J. Mat. Civ. Eng.* 32, 04020061. doi:10.1061/(asce)mt.1943-5533.0003136

Zhao, Y., Xiao, Z., Fan, C., Shen, W., Wang, Q., and Liu, P. (2020b). Comparative mechanical behaviors of four fiber-reinforced sand cemented by microbially induced carbonate precipitation. *Bull. Eng. Geol. Environ.* 79, 3075–3086. doi:10.1007/s10064-020-01756-4